



Published in final edited form as:

*Proc SPIE Int Soc Opt Eng.* 2020 February ; 11315: . doi:10.1117/12.2549041.

## Augmented reality visualization of hyperspectral imaging classifications for image-guided brain tumor phantom resection

James Huang<sup>1</sup>, Martin Halicek<sup>1</sup>, Maysam Shahedi<sup>1</sup>, Baowei Fei<sup>1,2,3,\*</sup>

<sup>1</sup>Dept. of Bioengineering, University of Texas at Dallas, TX

<sup>2</sup>Advanced Imaging Research Center, Univ. of Texas Southwestern Medical Center, Dallas, TX

<sup>3</sup>Dept. of Radiology, Univ. of Texas Southwestern Medical Center, Dallas, TX

### Abstract

Wearable augmented reality (AR) is an emerging technology with enormous potential for use in the medical field, from training and procedure simulations to image-guided surgery. Medical AR seeks to enable surgeons to see tissue segmentations in real time. With the objective of achieving real-time guidance, the emphasis on speed produces the need for a fast method for imaging and classification. Hyperspectral imaging (HSI) is a non-contact, optical imaging modality that rapidly acquires hundreds of images of tissue at different wavelengths, which can be used to generate spectral data of the tissue. Combining HSI information and machine-learning algorithms allows for effective tissue classification. In this paper, we constructed a brain tissue phantom with porcine blood, yellow-dyed gelatin, and colorless gelatin to represent blood vessels, tumor, and normal brain tissue, respectively. Using a segmentation algorithm, hundreds of hyperspectral images were compiled to classify each of the pixels. Three segmentation labels were generated from the data, each with a different type of tissue. Our system virtually superimposes the HSI channels and segmentation labels of a brain tumor phantom onto the real scene using the HoloLens AR headset. The user can manipulate and interact with the segmentation labels and HSI channels by repositioning, rotating, changing visibility, and switching between them. All actions can be performed through either hand or voice controls. This creates a convenient and multifaceted visualization of brain tissue in real time with minimal user restrictions. We demonstrate the feasibility of a fast and practical HIS-AR technique for potential use of image-guided brain surgery.

### Keywords

Augmented reality; hyperspectral imaging; image-guided surgery; brain tumor resection

## 1. INTRODUCTION

Image-guided surgery is especially important in brain tumor resection because it is imperative that as little of the brain is removed as possible. Successful resection of non-metastatic tumors has shown to significantly increase survival rates of brain cancer as well

\* bfei@utdallas.edu; Web: <https://www.fe-lab.org>.

as reduce the time required for adjuvant chemotherapy further down the line [1]. Despite this, brain tumor resections have historically been known to cause decreases in cognitive function and decision-making capacity due to excessive portions of the brain being removed. Cognitive deficiency as a result of brain tumor resection also raises the ethical issue of patients being unable to provide informed consent regarding their treatment [2]. Augmented reality and computer vision have been employed to address the challenges in brain surgery. However, current AR used in brain surgery is non-wearable and therefore an inconvenience for the surgeon in the operating room. During surgery, the surgeon must continuously switch between looking at the surgical field and computer screen, which disrupts the workflow and lengthens the procedure drastically [3]. Current augmented reality solutions for neurosurgery require several localization devices for spatial tracking and visualization, including cameras or 3D scanner, and computers for image rendering and display [4,5]. The equipment needs to be accurately placed and calibrated prior to surgery to ensure proper alignment and orientation of the augmented images [3]. When factoring in setting up, taking down, and transporting these AR systems, the surgical process is even further delayed. Wearable augmented reality is far less cumbersome and includes built-in simultaneous localization and mapping (SLAM) software, which generates a map of the environment and pinpoints the sensor location in that environment in real time [6]. This greatly expedites the calibration process as compared to contemporary AR-guided methods.

Hyperspectral imaging is an emerging technique and holds several advantages over other traditional imaging approaches. The most notable benefits to HSI as a form of optical imaging are its speed, cost, and size. A hyperspectral camera can be quickly transported between rooms and does not require specialized shielding and particle acceleration equipment [7]. Imaging, processing, and segmentation can be performed immediately before brain surgery, which reduces variability between acquisition and visualization. In neurosurgery, this is a critical aspect, as the brain shift phenomenon is known to void images taken pre-operatively very quickly [8]. The lesser known benefit to HSI is its customizability. Depending on the sensor used, an HSI camera can vary its spectral range to take images between 400 and 2500 nm, with certain wavelength ranges being better at identifying certain types of tissue [9]. Other features of a hyperspectral camera that can be easily interchanged to provide tissue images are the spectral light detector, dispersive device, acquisition mode, and measurement mode. For example, tumor hypoxia is best identified at a spectral range of 400 to 720 nm and when utilizing a liquid crystal tunable filter for dispersion, a staring acquisition mode, and fluorescence as the measurement mode [10]. Because the accuracy and precision of HSI can be manipulated by changing cameras and acquisition settings, HSI offers an extensive range of contrast mechanisms which can be applied to brain tissue classification [7,10].

By combining the various propitious qualities associated with wearable augmented reality and hyperspectral imaging, we aim to reach a new standard for image-guided surgery concerning accuracy, speed, and cost. The objective of the research was to minimize the error between the overlaid segmentations and the region of interest while greatly reducing the time between acquisition and visualization with a reasonable degree of correction for movement. We performed a tissue-based segmentation of an optical brain tumor phantom from its corresponding HSI hypercube using a neural network by examining the optical

properties of each tissue type. Then, we accurately superimposed the segmentation labels over the original phantom using a Unity script uploaded to the HoloLens. The designed joint HSI and AR surgical guidance system was tested for hologram registration accuracy through a series of positional and rotational tests. The following sections describe the HSI and AR systems as well as the experimental procedures.

## 2. METHODS

### 2.1 HSI Optical Phantom

An optical phantom was constructed to simulate biological tissue from material that mimics the optical properties observed. The phantom contained three different components to simulate each of normal brain tissue, blood vessel, neoplasm or tumor. The tumor phantom component, which was denser and stiffer as opposed to the rest of the phantom material, was composed of 4% agar, 2% bovine gelatin (Sigma Aldrich, Ann Arbor, MI, USA), and 20  $\mu\text{L}$  of yellow pigment ink. The tumor phantom was allowed to solidify at room temperature in a well-plate. The phantom was then placed in a petri dish, which served as the main mold for the phantom. The brain tissue phantom component was added to the petri dish and was composed of a gelatin solution that was 3% agar and 1.5% bovine gelatin. The blood vessel component of the phantom was constructed by boring out channels in the main phantom and filling it with a gelatin solution composed of 10% porcine whole blood (Lampire Biological Laboratories, Pipersville, PA, USA), 3% agar, and 1.5% bovine gelatin. After the phantom completely solidified at room temperature, the phantom was placed inside a cavity formed above the ear of the foam manikin head, and HSI were acquired of the phantom *in-situ*.

### 2.2 HSI Calibration and Acquisition

As shown in Figure 3, the HSI data was acquired from the optical phantom using a customized hyperspectral system from 485 to 900 nm in 2.5 nm intervals to produce an HSI hypercube with 150 spectral bands. The image size of the HSI was 1088 by 2048 pixels, and the imaging time was about 40 seconds. The system was adjusted to use a staring acquisition mode and reflectance measurement mode. Calibration of the hyperspectral system was performed by placing a black and white checkerboard pattern on the head model. By applying the known black and white colors as well as the size of the checkerboard as the standards, the application settings were tuned accordingly to establish the exact distance and orientation of the phantom from the camera and the necessary lighting adjustments for the environment. A slightly more reflective material was chosen for the checkerboard to be printed on in order to better represent the glossy, highly reflective surface of the brain tumor phantom. The checkerboard was procedurally scanned to generate a panorama-like image (Figure 3), and the acquisition speed of the system was adjusted until the sections of the checkerboard appeared perfectly square on the display.

### 2.3 Image Classification

The files were loaded into MATLAB (MathWorks Inc, Natick, MA, USA), where a simple neural network with one hidden layer and 48 nodes was trained on regions of the three components of the HSI from the phantom. The entire HSI was classified using this neural network to generate predicted areas of normal brain tissue, blood vessel, and tumor. While

the tumor was constructed using the same material as the simulated normal tissue, the optical properties observed of each were shown to be fundamentally different. It was found that the most propitious region for distinguishing normal brain tissue (gelatin) from tumor (yellow) was 485 to 510 nm.

## 2.4 Phantom Tracking Techniques

To track the phantom, we employed the AR SDK Vuforia, which uses a feature-based registration method to determine the position and orientation of the phantom and anchor holograms to it. Features in AR terms are the sharp edges and highcontrast points in an image or object which are easily distinguishable from their immediate surrounding area [11]. The features of the brain tumor phantom were extracted from its RGB image using the Vuforia developer portal, and its suitability as a tracking target was assessed. In previous iterations of the experiment using agarose gel and representative colored dyes for blood vessels and tumors, it was found that the phantom itself was often insufficient for a stable and accurate tracking scene. This is caused by the onboard camera's inadequate resolution and high sensitivity to glare, two shortcomings of current wearable AR headsets.

The tracking issue was addressed by implementing a second, default tracking target provided by Vuforia, to serve as a reference to re-stabilize the scene when tracking of the phantom was lost. This default target had the ideal number of features, 300+, compared to the ~40 of the brain tumor phantom, and was mounted on a frame surrounding the circular phantom.

## 2.5 Application Building and Deployment

Each dataset that was pertinent to the specific trial was loaded into Unity (Unity Technologies, San Francisco, CA, USA), including the array of hyperspectral images, the segmentation labels, and the RGB phantom image for tracking. This process was performed manually, but the application can support any number of bands and segmentation images. The application automatically handled the alignment and scaling of the holograms in relation to the phantom through a script. A color-based pixel separation script was used to further differentiate the tissue of interest from the other tissue in each segmentation image. For each segment, the background alpha value was changed to 0 to make it completely transparent, leaving only the pixels from the tissue of interest visible. This made it possible to view the segmentation holograms overlaid on the phantom without obscuring the rest of it. A mask was generated through a script to crop the band images and segmentation labels to display only the phantom and not the surrounding area in the holograms. Following these simple preliminary steps of loading the hypercube and segmentation labels and RGB composite image into the scene, the Unity project was built for the Universal Windows Platform and deployed to the HoloLens AR headset (Microsoft, Redmond, WA, USA), either through Wi-Fi or cable.

The AR application was composed of three different phases; localization, calibration, and tracking. In the localization phase, the HoloLens utilized SLAM to generate a spatial mesh of the environment to establish collision detection and attempted to find the phantom and the tracking target. Once the position of the targets was determined, a calibration hologram was anchored to the phantom in a presupposed location, centered on the phantom and floating

0.1 mm above it. The user was then guided through several steps to make small adjustments to the tilt and position of the holograms to account for the imperfections caused by headset orientation. Auxiliary markers and a holographic axis made the alignment process much easier. After calibration, the targets were ready to be tracked and the menus for the various options for hologram manipulations was displayed.

### 3. RESULTS

Figure 8 demonstrates the anticipated scene setup in the operating room, with the surgeon viewing the real-time tissue segmentations for image-guided surgery or training through the HoloLens. The top and bottom right images show the holographic scene, or what the surgeon would be seeing through the headset. The two panels shown in the bottom right allow the user to switch between each of the hyperspectral band images and choose which of the three tissue segmentations to overlay by checking their respective boxes.

The accuracy test procedure consisted of recalibration with respect to the orthographic top view at  $0^\circ$ , followed by measuring the error along x- and y-axes at each of the isometric top views ( $0 - 325^\circ$  in  $45^\circ$  increments), the error along z-axis at each of the orthographic side views, and the error along x-, y-, and z-axes for each of the isometric views. The orthographic view refers to the two-dimensional representation of the wooden frame, either from the side or from a bird's eye view, and the isometric view refers to what a person would see when standing off to the side and looking down at an object. The bottom left image in Figure 8 provides a working example of the isometric view.

The accuracy test results were obtained by overlaying the phantom with a printout of a  $1 \times 1$  mm grid and placing a pink holographic axis (Figure 9) at the center of the projected images. The orthographic accuracy was assessed in the top-down configuration for the x and y axes and in the side configuration for the z-axis. The accuracy of the application was also evaluated in the isometric configuration, in which the user stood straight up and looked at the image target from a short distance away. The z-axis offset was measured using a ruler placed normal to the grid plane, while the x and y axes errors were measured by looking at the printed grid and recording the position of the holographic axis origin in relation to it. Measurements were taken from eight positions surrounding the image target for a total of 16 error values for each of the axes. Five trials were performed with two different subjects wearing the headset. All measurements were done in millimeters. The accuracy results can be seen in Table 1.

### 4. DISCUSSION AND CONCLUSION

In this study, we developed a hyperspectral imaging augmented reality system for image-guided surgical applications. The incorporation of HSI into AR presents a very fast alternative for brain tumor visualization and resection guidance.

While some processes regarding the HSI visualization in AR can be expedited through user familiarity, other aspects, such as the act of image acquisition and image processing hold a fixed amount of time. For example, the hyperspectral system used has a one-minute runtime and the Unity build and deployment to HoloLens through Visual Studio 2017 took a few

minutes for each trial that was run. These are inflexible hurdles for real-time visualization of brain tumors, and it is dubious whether the procedure can be shortened significantly in the near future. Most of the difficulties we ran into during this project could be attributed to the hardware of the Microsoft HoloLens, which is still lacking in terms of memory, stability, and image capture quality. The large variations in registration error, especially in the y-direction, are a result of the HoloLens' inadequate spatial awareness, and holograms shifting positions over time in the operating room would be a major hazard when combined with natural organ shifting and deformation [12]. The pixel separation script, mentioned in section 2.4, took approximately a minute per segmentation image due to unoptimized implementation and insufficient onboard RAM. In terms of presenting results as seen through the HoloLens, the mixed reality capture utilizes a different camera of the three onboard the HoloLens than the one used for tracking, and therefore it was not possible to record exactly what the user was seeing, only an offset representation of it.

Nonetheless, contemporary wearable AR systems are still lacking in terms of stability and tracking capabilities and are therefore only suitable for training and simulation purposes. With the current focus of AR development on industry rather than medical use, this issue may take some time to be resolved. However, with further improvements in AR technology, wearable AR will undoubtedly become a new tool for image-guided surgery procedures.

In conclusion, we introduced the integration of hyperspectral imaging with augmented reality and examined its capacity as a real-time brain tumor visualization method as well as its shortcomings. Additionally, we designed a novel optical phantom for hyperspectral imaging which could be used for neural network training and improving segmentation algorithms. The results for tissue classification using the optical brain tumor phantom have been promising. As a byproduct of our studies, we were able to gauge the efficacy of the HoloLens and the auxiliary tracking software Vuforia as a visualization modality as well.

## ACKNOWLEDGMENTS

The authors would like to thank Patric Bettati for his contribution in accuracy measurement experiment. This research was supported in part by the U.S. National Institutes of Health (NIH) grants (R01CA156775, R01CA204254, R01HL140325, and R21CA231911) and by the Cancer Prevention and Research Institute of Texas (CPRIT) grant RP190588.

## REFERENCES

- [1]. Parrish-Novak J, Holland EC and Olson JM, "Image Guided Tumor Resection," *The Cancer Journal*, vol. 21, no. 3, pp. 206–212, 2015. [PubMed: 26049700]
- [2]. Veretennikoff K, Walker D, Biggs V and Robinson G, "Changes in Cognition and Decision Making Capacity Following Brain Tumour Resection: Illustrated with Two Cases," *Brain Sciences*, vol. 7, no. 10, pii: E122, 2017. [PubMed: 28946652]
- [3]. Tagaytayan R, Kelemen A and Sik-Lanyi C, "Augmented reality in neurosurgery," *Archives of Medical Science*, vol. 14, 2018.
- [4]. Shuhaiber JH, "Augmented reality in surgery," *Jama Surgery*, vol. 139, no. 2, pp. 126–132, 2004.
- [5]. Liao H, Inomata T, Sakuma I and Dohi T, "3-D Augmented Reality for MRI-Guided Surgery Using Integral Videography Autostereoscopic Image Overlay," *IEEE Transactions on Biomedical Engineering*, vol. 57, no. 6, pp. 1476–1486, 2010. [PubMed: 20172791]

- [6]. Grasa OG, Civera J and Montiel JMM, "EKF monocular SLAM with relocalization for laparoscopic sequences," in IEEE International Conference on Robotics and Automation, Shanghai, 2011.
- [7]. Hillman EMC, "Optical brain imaging in vivo: techniques and applications from animal to man," *Journal of Biomedical Optics*, vol. 12, no. 5, p. 28, 2007.
- [8]. Fabelo H, Halicek M, Ortega S, Shahedi M, Szolna A, Piñeiro JF, Sosa C, O'Shanahan AJ, Bisshopp S, Espino C, Márquez M, Hernández M, Carrera D and Morera J, "Deep Learning-Based Framework for In Vivo Identification of Glioblastoma Tumor using Hyperspectral Images of Human Brain," *Sensors*, vol. 19, no. 4, pii: E920, 2019. [PubMed: 30813245]
- [9]. Halicek M, Fabelo H, Ortega S, Callico G and Fei B, "In-Vivo and Ex-Vivo Tissue Analysis through Hyperspectral Imaging Techniques: Revealing the Invisible Features of Cancer," *Cancers*, vol. 11, no. 6, pp. 756, 2019.
- [10]. Lu G and Fei B, "Medical hyperspectral imaging: a review," *Journal of Biomedical Optics*, vol. 19, no. 1, pp. 010901, 2014.
- [11]. Ibañez AS and Figueras JP, "Vuforia v1.5 SDK: Analysis and evaluation of capabilities," Polytechnic University of Catalonia, Barcelona, 2013.
- [12]. Chen L, Day TW, T. W. and John NW, "Recent Developments and Future Challenges in Medical Mixed Reality," in 2017 IEEE International Symposium on Mixed and Augmented Reality, Nantes, 2017.

## Augmented Reality HSI Surgical Guidance

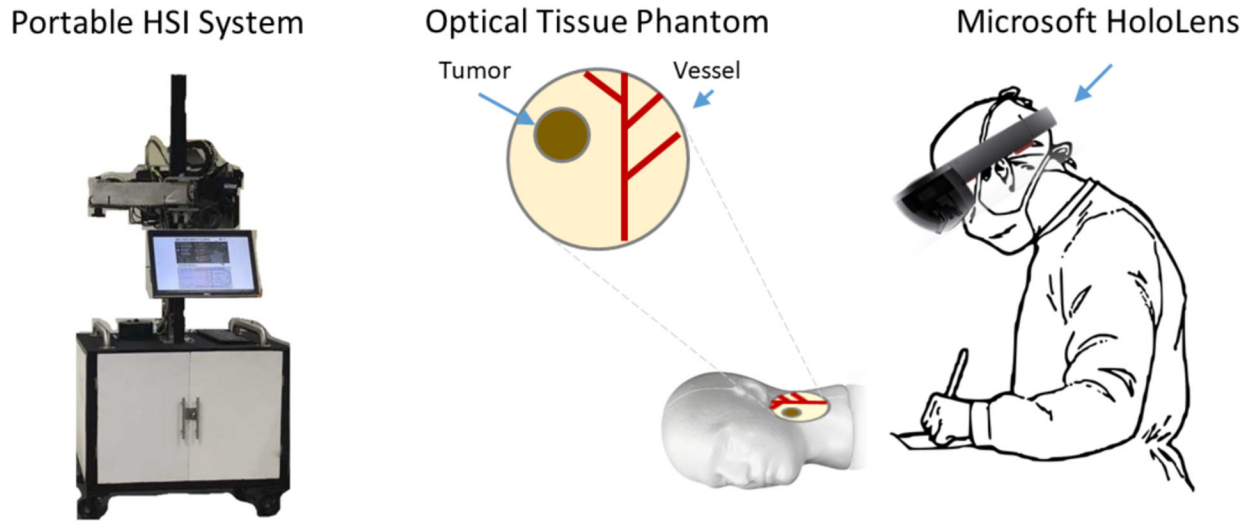


**Figure 1.**

The three main components of the AR surgical guidance experiment were the portable hyperspectral imaging system, the optical tissue phantom, and the Microsoft HoloLens. The HSI system was used to first generate the hypercube of the optical tissue phantom over a specific wavelength. Then, the hyperspectral images were classified into three types of tissue: tumor, blood vessel, and normal brain tissue. Finally, the HoloLens was loaded with an application to allow a surgeon to view the hyperspectral images and tissue segmentations overlaid on the phantom in real time.

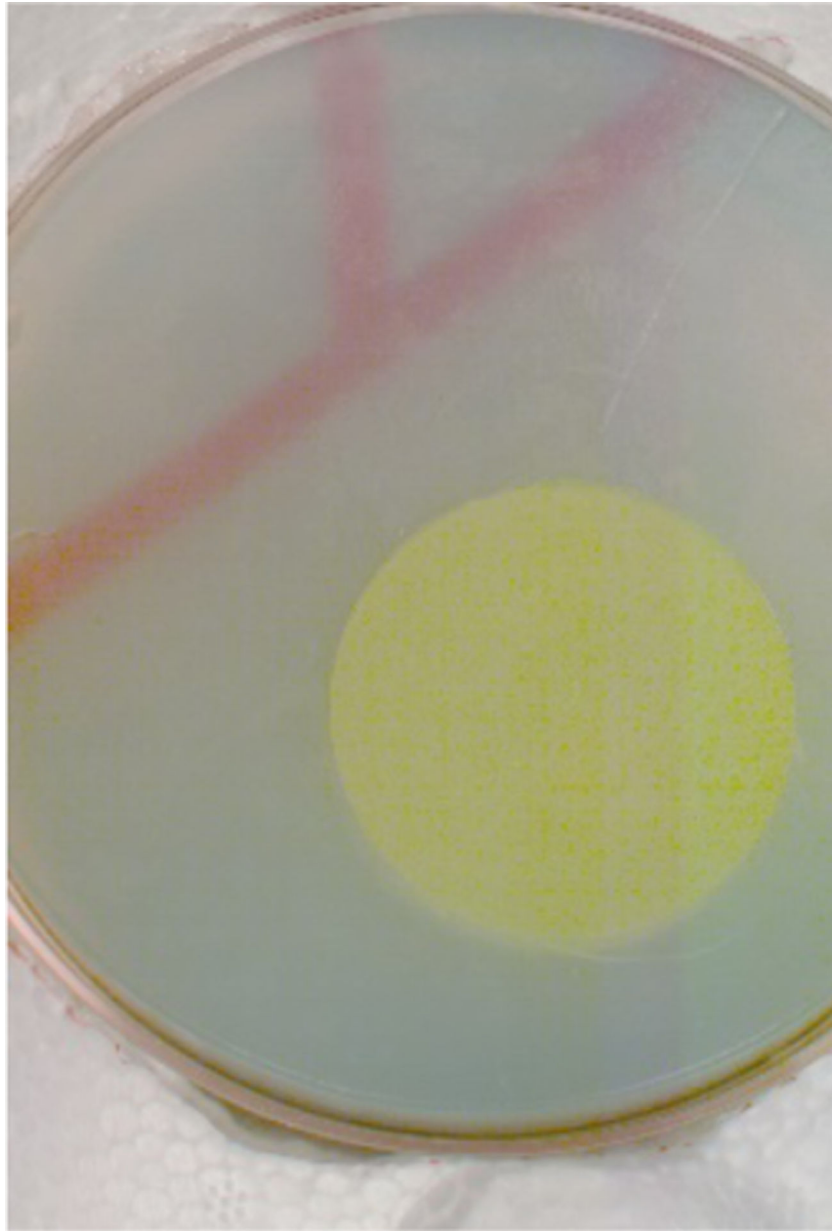


**Figure 2.**

A brain tumor phantom was built for the purposes of hyperspectral imaging testing and classification. The blood is shown in red, the normal brain tissue is the translucent material, and the tumor or neoplasm is shown in yellow. Blood is most visible in the 500 to 600 nm range, while the benign tumor tissue was made stiffer and denser compared to the other tissue to simulate angiogenesis. In this way, we were able to imitate some of the properties of the real tissue using a phantom.

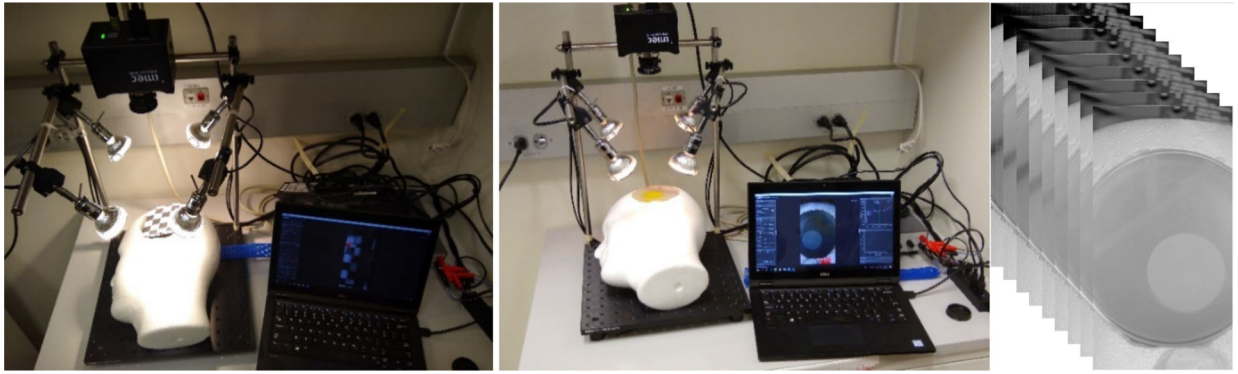


**Figure 3.**

The calibration and acquisition processes were performed in the same location on the head model under the same illumination conditions. The image on the left demonstrates the alignment process of the HSI system using a checkerboard. An expanded, panorama-like image was generated as the checkerboard was procedurally scanned and the speed of the camera's movement across the support beam was adjusted until the sections of the checkerboard appeared perfectly square on the display. This takes approximately 40 seconds. In the center, the setup for HSI acquisition of the brain tumor phantom is shown. On the right, a sample of 9 spectral bands from the generated 150 band HSI hypercube is displayed.

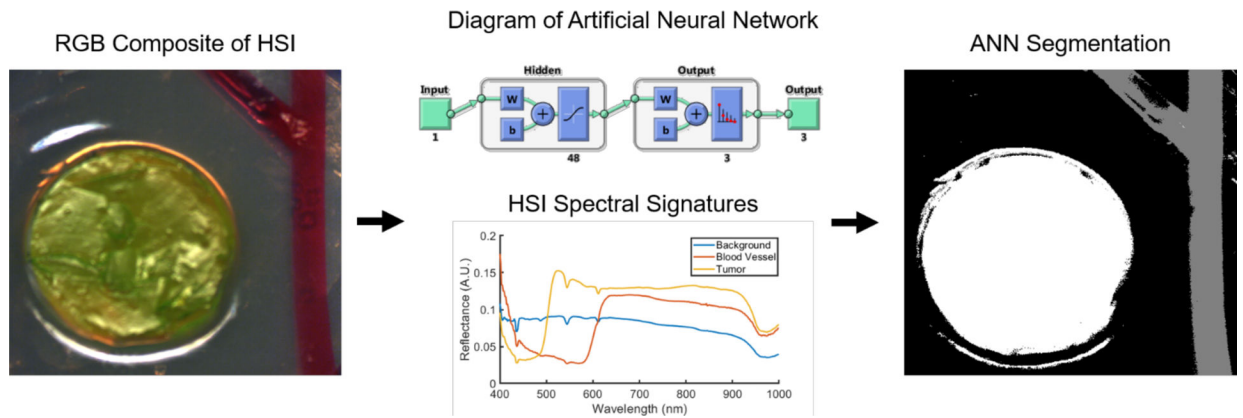


**Figure 4.** The image classification process was performed by training an artificial neural network on the three regions of the RGB composite image of the phantom’s HSI by extracting each region’s spectral signature, or reflectance values over the wavelength range. Next, the HSI hypercube was used to sort the images pixel by pixel into the three regions until the image was fully segmented into normal tissue, blood vessel, and tumor.

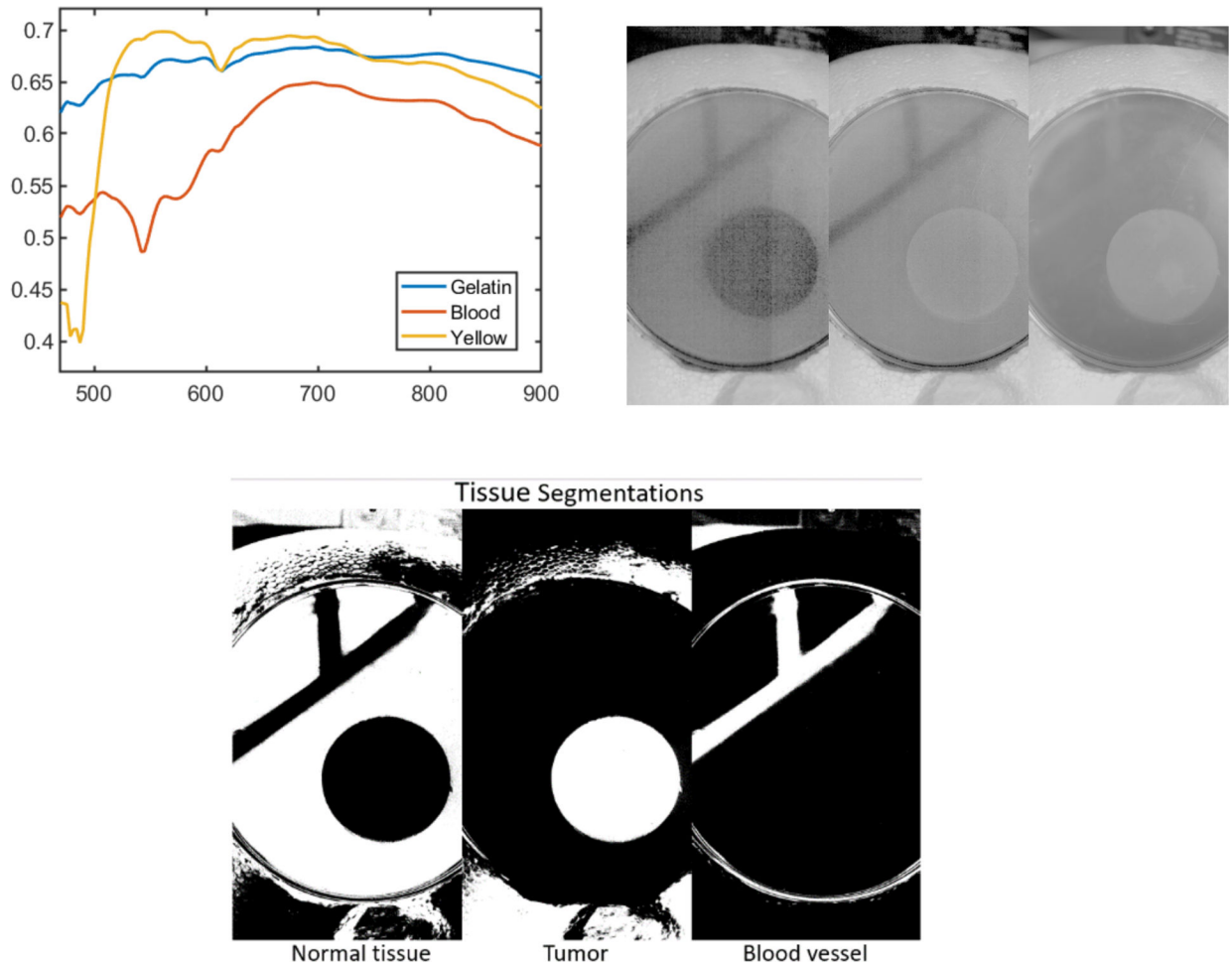


**Figure 5.**

Generating the reflectance spectra of the three tissue types revealed certain characteristics of each one and made it easy to classify the tissues. On the left is the HSI reflectance spectral signature plot for three simulated tissue types, with gelatin representing normal brain tissue and yellow representing tumor. Aside from the yellow dye, the tumor is comprised of the same material as the normal brain tissue, but there exists a very noticeable difference between the reflectance spectra of the two. On the top right, Spectral Band 5 at 500 nm (left) is shown next to Band 15 at 525 nm (center) and Band 145 at 850 nm (right) for comparison purposes. In Band 15, the porcine blood is clearly visible but fades away as the reflectance increases in Band 145. At wavelengths lower than 510 nm as in Band 5 of 500 nm (left), the tumor was seen to have a significant drop in its reflectance value. The bottom image shows the segmentation labels of the phantom for each tissue type.

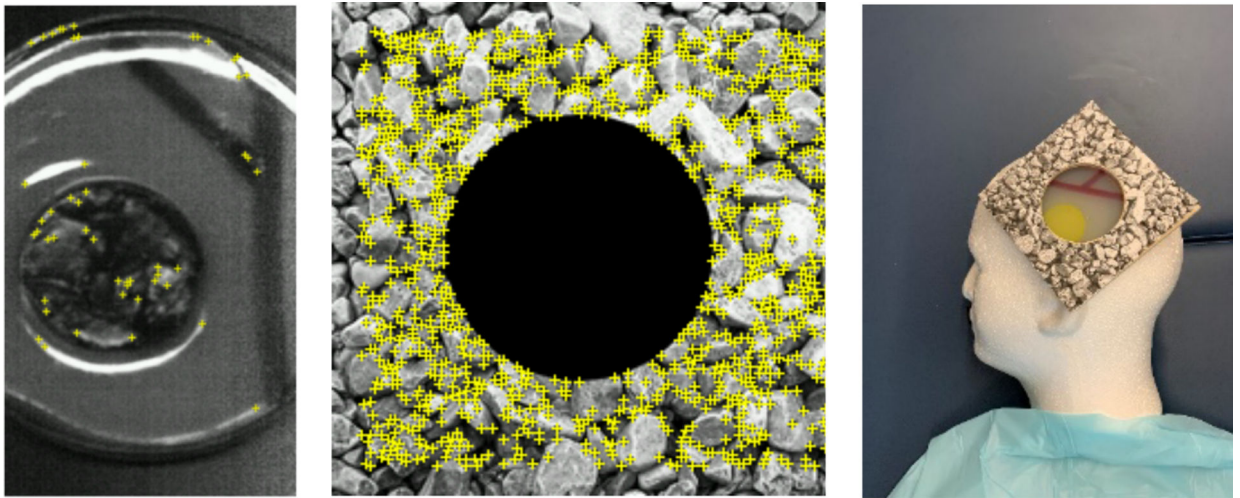


**Figure 6.**

A supplementary tracking target with a viewing portal was positioned above the brain tumor phantom to allow for robust registration of holograms. On the left is the optical phantom with its features extracted by Vuforia overlaid by yellow cross symbols. In the center is the tracking target image with its extracted features by Vuforia overlaid by yellow cross symbols. It is evident from the images that the ideal image was far more suitable for tracking purposes than the RGB image of the phantom because it had more sharp edges and corners rather than circles and straight lines. To add the target to the scene, a printout of the image was mounted to a wooden frame, which was positioned on the head model and fastened in place.

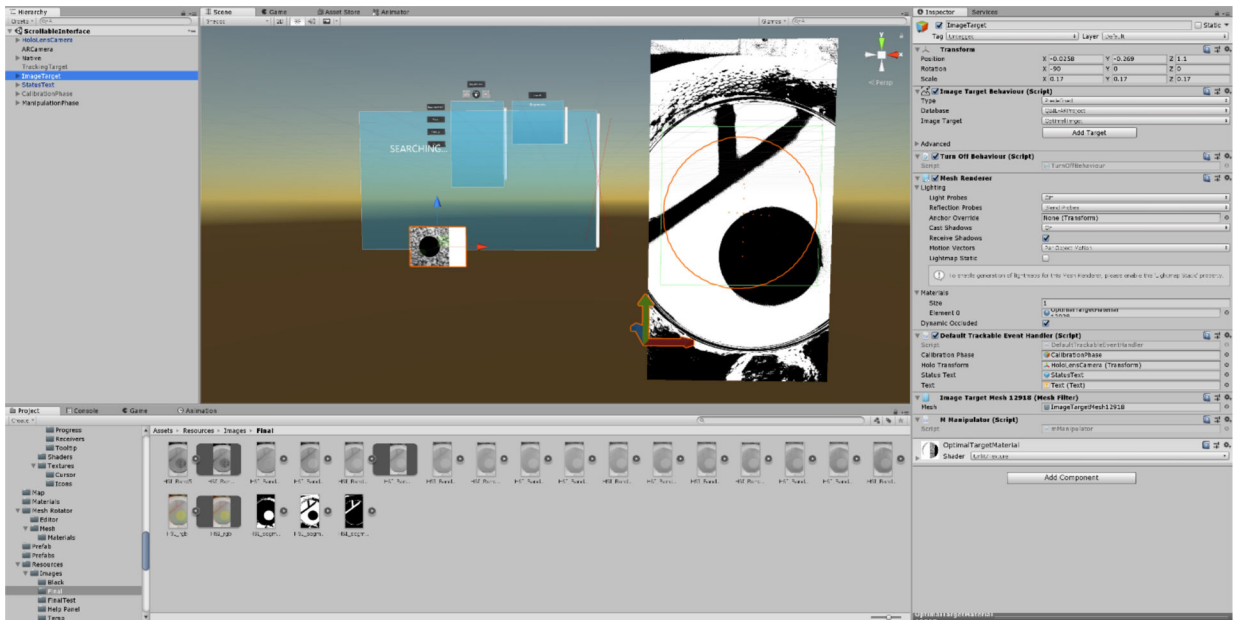


**Figure 7.** The augmented reality software interface system. The application required various inputs from the user including the HSI hypercube, the tissue segmentations, and the RGB composite image of the phantom for tracking. The hypercube and tissue segmentations were loaded into their corresponding folders in the Unity scene which the scripts called from and the RGB image was entered into its corresponding data field. The positioning and sizing of the holograms was then handled automatically through a script.

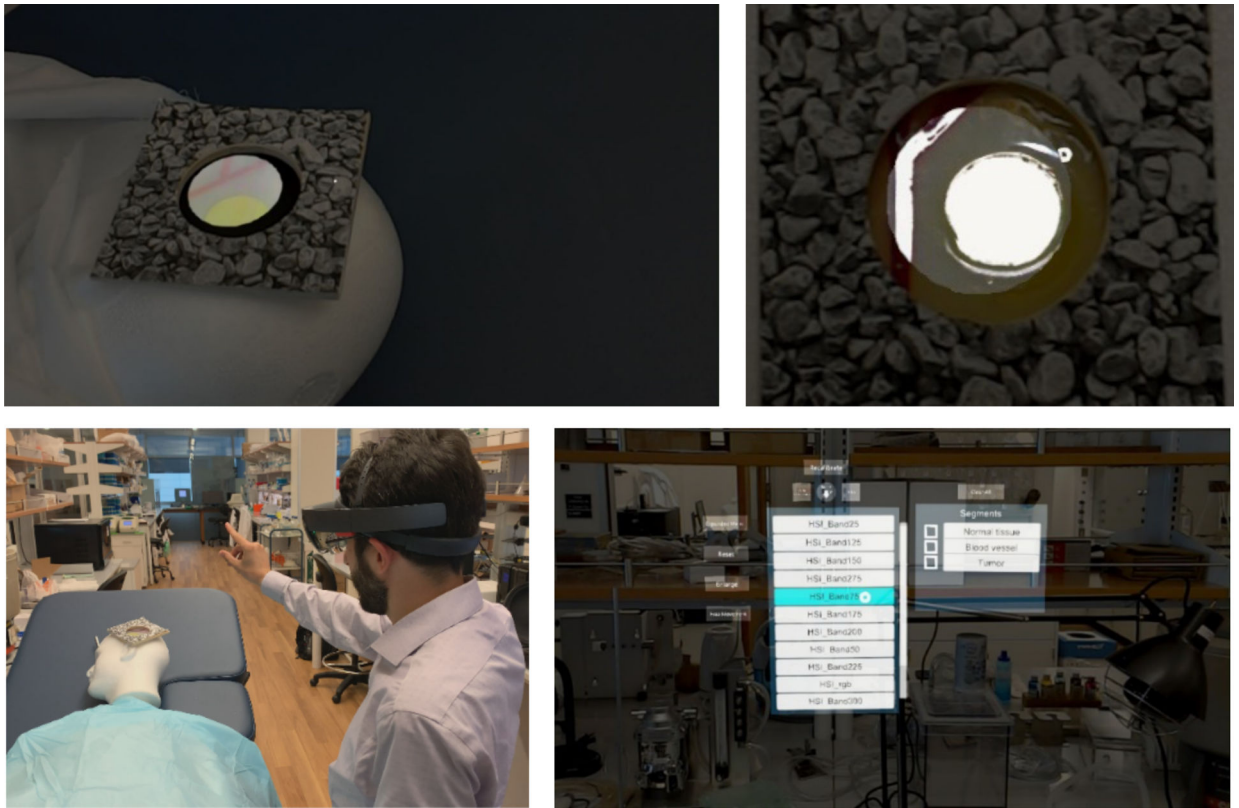


**Figure 8.**

The HoloLens application creates a convenient and untethered method to visualize tissue segmentations in real time. The top two images shows the segmentation labels overlaid on top of the brain tumor phantom. From the images, it can be seen that the boundaries of the blood vessel and tumor are clearly defined and easily distinguishable from the surrounding tissue. The image on the bottom left shows the scene setup and basic interaction with the application through a finger tap movement. On the bottom right is the application interface as seen through the HoloLens. There is a band selection menu which contains each of the spectral bands in the hypercube as well as a smaller segmentation label menu which allows the user to see the tissue segmentations overlaid on the phantom.

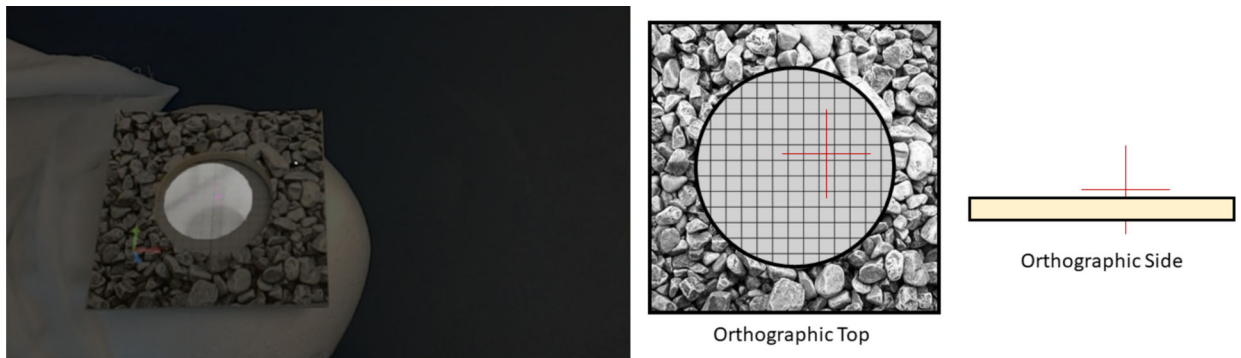


**Figure 9.**

Accuracy tests were performed on the hologram registration scene to quantify the error in the x, y, and z directions. The left image shows the setup for the test with the holographic axis in pink and the printed grid underneath the tracking target frame. It also represents the position for an accuracy test for the isometric view at 0 degrees. On the right, examples of the orthographic top and side views along with the holographic axis are shown to aid in visualization of how the accuracy test was done.

**Table 1.**

Registration error in mm from isometric and orthographic views in the X, Y, and Z directions presented as Mean +/- Standard Deviation over 5 trials.

View	X	Y	Z
Isometric	$1.75 \pm 1.97$	$4.80 \pm 2.17$	$0.70 \pm 0.80$
Orthographic	$2.13 \pm 1.59$	$4.33 \pm 4.13$	$0.75 \pm 0.84$